Inorganic Chemistry

Article

pubs.acs.org/IC

Halide Binding and Inhibition of Laccase Copper Clusters: The Role of Reorganization Energy

Kasper P. Kepp*

DTU Chemistry, Technical University of Denmark, Building 206, 2800 Kgs. Lyngby, DK Denmark

Supporting Information

ABSTRACT: Laccase-like proteins are multicopper oxidases involved in several biological and industrial processes. Their application is commonly limited due to inhibition by fluoride and chloride, and as-isolated proteins are often substantially activated by heat, suggesting that multiple redox states can complicate characterization. Understanding these processes at the molecular level is thus desirable but theoretically unexplored. This paper reports systematic calculations of geometries, reorganization energies, and ionization energies for all partly oxidized states of the trinuclear copper clusters in realistic models with ∼200 atoms. Corrections for scalar-relativistic effects, dispersion, and thermal effects were estimated. Fluoride, chloride, hydroxide, or water was bound to the T2 copper site of the oxidized resting state, and the peroxo intermediate was also computed for reference. Antiferromagnetic coupling, assigned oxidation states, and general structures were consistent with known spectroscopic data. The computations show that (i) ligands bound to the T2 site substantially increase the reorganization energy of the second reduction of the resting state and reduce the redox potentials, providing a possible mechanism for inhibition; (ii) the reorganization energy is particularly large for F^- but also high for Cl^-, consistent with the experimental tendency of inhibition; (iii) reduction leads to release of Cl^- from the T2 site, suggesting a mechanism for heat/reduction activation of laccases by dissociation of inhibiting halides or hydroxide from T2.

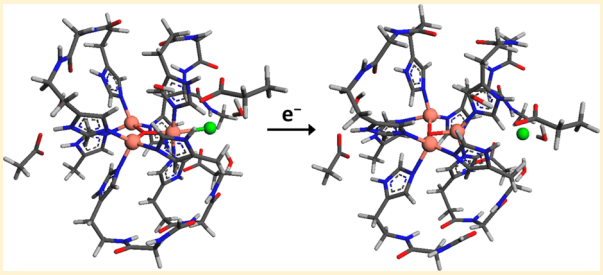

INTRODUCTION

Laccase-like multicopper oxidases all have cupredoxin-type domains and copper sites that enable enzymatic oxidation of chemically diverse substrates such as inorganic metal ions,[1,2] bilirubin,[3,4] complex phenols and amines, and redox mediators.[5−8] Their superior oxidation power, broad activity, and high stability have led to numerous technological applications including bioremediation,[9] lignin degradation,[10,11] and industrial bleaching.[12,13]

The most commonly studied three-domain laccase-like proteins contain four copper ions: The T1 copper site is coordinated by two histidine residues and one cysteine, sometimes with an additional methionine, and is situated close to the substrate that is oxidized by electron abstraction. 10−15 Å from this copper, a dinuclear coupled T3 site coordinated by histidines is positioned in close contact with a fourth T2 copper: These three copper ions constitute a trinuclear cluster (TNC) that is responsible for four-electron reduction of oxygen to water, using electrons supplied by the T1 site by intramolecular electron transfer.[14−16]

Laccase-like proteins are commonly inhibited by small halides such as fluoride and chloride, which bind to the T2 copper,[17,18] and fungal laccases are most active at low pH where they are also less stable; these difficulties have spawned efforts to improve the tolerance of laccases to wider ranges of pH and ionic strength[19] and identify new halophilic laccase-like proteins.[20,21] Bacterial laccase-like proteins offer major potential in this direction due to their high stability and sequence diversity.[22−24] Several protein states have been observed for laccase-like proteins, first for bilirubin oxidase.[25] As-isolated laccase-like proteins such as bilirubin oxidase from *Myrothecium verrucaria* and CotAs from the genus *Bacillus* are subject to substantial heat activation that increases protein turnover and alters spectroscopic properties.[8,25−27] Chemical reduction has been found to enable conversion of an as-isolated alternative resting state of bilirubin oxidase into another resting oxidized state, which was 10-fold more active.[28]

Given the importance of these several states in characterization and use of laccase-like proteins, and due to the potential biological role of such states, it is of interest to understand the mechanism behind both general laccase inhibition by small halides and the inactivation−activation processes that can be caused by heat and reducing agents. This paper reports density-functional studies of realistic models of the TNCs based on the crystal structure of the archetypical bacterial CotA,[29] involving all important second-sphere interactions and variable ligands bound to the T2 site; this model is shown in Figure 1, left, and the general reaction scheme is shown in Figure 1 right, where this study focuses on modified states in the lower left. All partly oxidized redox states and ferromagnetically coupled states were geometry optimized to give insight into the effect of reduction

Received: September 5, 2014
Published: December 23, 2014

DOI: 10.1021/ic5021466
Inorg. Chem. 2015, 54, 476−483

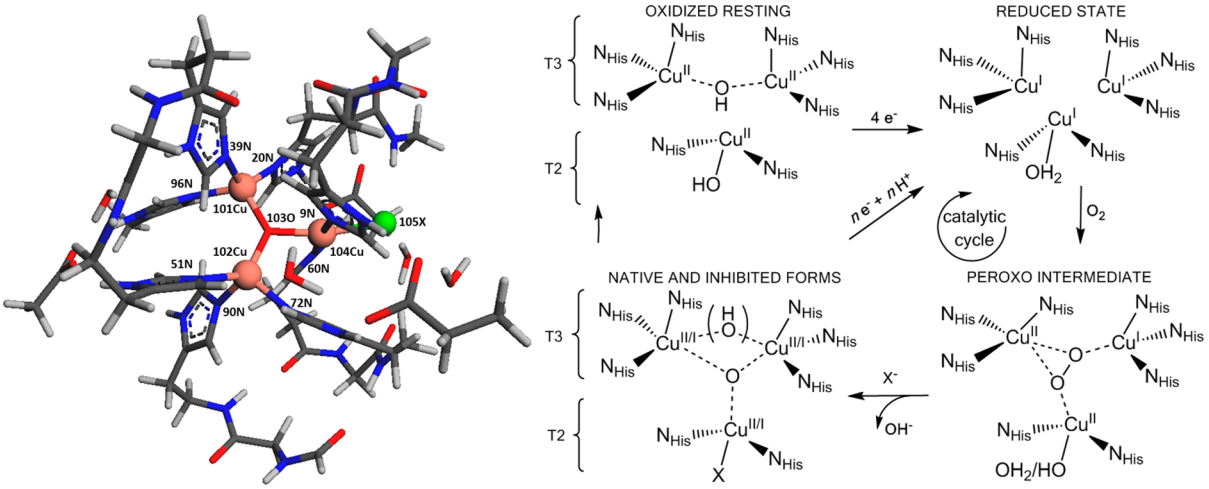

Figure 1. (left) General model and numbering scheme used in this work: Ligand 105X = Cl^-, H_2O, F^-, or OH^-. 103O = O^{2-} or O_2. All one-, two-, or three-electron oxidized combinations of spin and oxidation states were computed. The Figure was made using ArgusLab 4.01. (right) General reaction scheme for the trinuclear cluster of laccase-like proteins (ref 14); the present work focuses on the bottom two parts. The NI is the form in the lower left with all three Cu(II), with X = OH^-, and with the hydroxo bridge present. Other partly reduced versions of both the PI and inhibited forms were studied in the present work.

as a reactivation step, directly rationalized by the electronic energies of the trinuclear cluster of these proteins.

METHODS

Chemical Models. The models were constructed from the crystal structure 1GSK.pdb of CotA from *B. subtilis* at a resolution of 1.70 Å.[29] In this structure, consistent with the current view of the resting oxidized (RO) state of these proteins,[14] a solvent (hydroxide) is coordinated to the T2 site. An oxide ion resides within the T3 site with Cu−O distances of 2.11 and 2.19 Å, which is distinct from the μ_3-oxo structure deduced for the native intermediate (NI).[14] The computed RO state (i.e., the II,II,II state with OH^- bound) started from the 1GSK structure converted into a μ_3-oxo structure upon optimization in all cases, consistent with the consensus view of this state.[14] Because of the resolution, it is not possible to distinguish the protonation state directly from the structure; however, inspection of the oxygen atom indicates little room for a proton near the coppers, consistent with an RO state where the coppers are all Cu(II), to give these four atoms a total charge of +4 and an unfavorable free energy of protonation (this can be compared, e.g., to +3 hexaqua complexes that have $pK_a < 7$). Consistent with this, the catalytically relevant NI (but not the RO) has been assigned as fully deprotonated oxide.[14] The T2 solvent water is generally considered to be in the form of a hydroxide.[14] However, for completion, this state was computed both with H_2O and OH^- bound as the T2 ligand (representative structures can be viewed in Supporting Information, Figure S1).

Importantly, bacterial laccase-like proteins such as the spore-coat CotA proteins differ relative to the fungal counterparts, notably in the T1 site (having the classical 2His, 1Met, 1Cys motif, where fungal laccases typically miss the Met and associated lone pair electron density, contributing to their larger redox potentials.[14,15]

Eight histidines (105, 107, 153, 155, 422, 424, 491, 493) coordinate to the coppers. Two conserved aspartates (Asp116 and Asp465, corresponding to Asp77 and Asp424 in the fungal *Trametes versicolor* laccase structure 1GYC.pdb) hydrogen bond to two of the histidines (His424, 2.70 Å and His107, 3.64 Å) and are within ∼6 Å of the T2 copper. Since these affect the ligand field strength and Cu−N distances of the histidines, and Asp116 has been shown by site-directed mutagenesis to be required for reactivity,[30] these two side chains were included in the models.

Water molecules are located close to the TNC at several positions in strong hydrogen bonding interaction with ligands bound to the coppers: One water is located close to the T3 oxygen at only 3.06 Å, which thus needs to be included in any modeling of these states. Also, there are two water molecules hydrogen bonding to the T2 ligand at 2.75 Å (HOH2153 and HOH2416) that are required in a realistic model. Six of the eight histidines coordinating to copper in the TNC are connected by short backbone segments, and full inclusion of these three segments enables preservation of the protein backbone structure without overconstraining the residues to fixed positions; this is important since major reorganizations occur during ligand binding and redox chemistry, for example, ∼0.5 Å variation in Cu−Cu distances between the various states.[14] The backbone NH of Gly108 also hydrogen bonds to the T2 ligand critical to this study, so this part of the Gly108 backbone was also included in the models.

All partially oxidized states with either F^-, Cl^-, OH^-, or H_2O bound to the T2 copper of the RO state were studied, to identify possible structures of inhibited intermediates and alternative redox states that could explain experimental data. In addition, the peroxo intermediate (PI) was also studied in the form consistent with the current view on this state,[14] that is, with a peroxide bound to the T3 site with oxidation state II,II,I for the TNC. This state was first described in molecular detail by Rulisek et al. using QM/MM models with first-sphere QM models of 80−87 atoms that allowed an exhaustive investigation of the energetics of possible states and provided detailed suggestions for the involved states.[31] The models used here had total charges varying from −2 to +1, depending on ligand and redox state and included from 203 (the halide models of the resting oxidized state) to 206 atoms (the peroxo intermediate). Molecular orbitals were visualized using gOpenMol version 3.0 (by Leif Laaksonen, Center for Scientific Computing, Espoo, Finland) with plt files generated from Turbomole property ridft runs (additional MOs are shown in Supporting Information, Figures S2 and S3).

Geometry Optimizations. The calculations were performed with the Turbomole 6.3 software.[32] All models were studied both in the fully oxidized states and in the one- or two-electron reduced states relevant to the first turnovers that produce alternative resting states and inactivated laccase states. (In contrast, the fully reduced states is readily active and does not represent any inhibited form; thus, it was omitted from the current study.) Also, in all cases, both the high-spin ferromagnetic coupled state (M_S = 1 or 3/2) and the antiferromagnetic coupled state (M_S = 0 or 1/2) were subject to full geometry optimization, since all antiferromagnetic coupled state calculations were started from the ferromagnetic coupled states to facilitate convergence. Thus, in total, 30 systems were optimized. The fully optimized structures are given for reproducibility as xyz coordinates in the Supporting Information.

DOI: 10.1021/ic5021466
Inorg. Chem. 2015, 54, 476−483

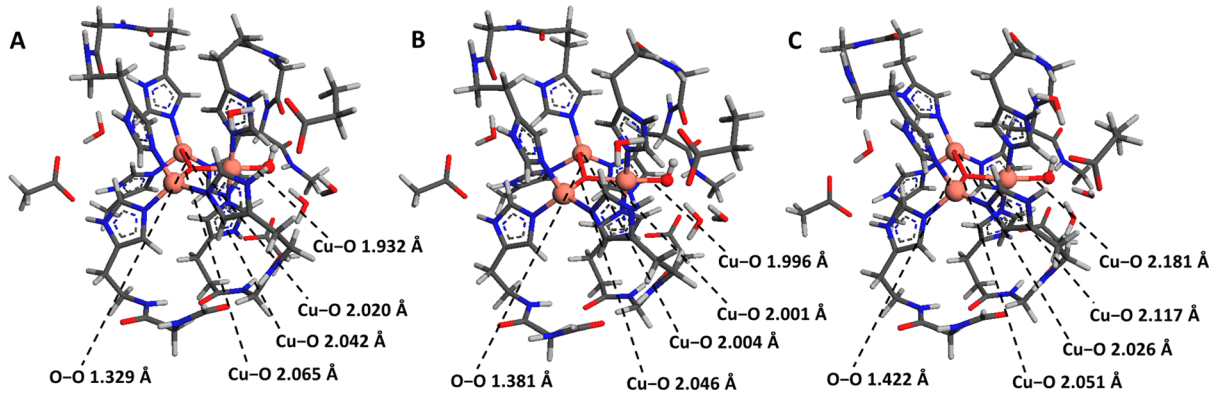

Figure 2. Optimized structures of (A) the one-electron oxidized form of the peroxo intermediate with (II,II,II) redox state, (B) the peroxo-intermediate with (II,II,I) redox state, and (C) the one-electron reduced peroxo intermediate (PI + e^-). Figure made with ArgusLab 4.01.

Optimization of all geometries were performed at the BP86/def2-SVP level[33] using the Cosmo solvation model[34] with dielectric constant 10, since condense phase screening has been shown to improve the accuracy of geometries of charged metal clusters versus experimental data.[35] The default optimized radii of 2.0 Å for C, 1.83 Å for N, 1.72 Å for O, 1.3 Å for H, and 2.0 Å for Cu. Electronic energies were converged to 10^{-7} a.u., and during geometry optimization, the gradient of the energy was converged to 10^{-3} a.u.

Energy Calculations. After convergence of all geometries, the energies of each state were computed again with a larger, polarized basis set def2-TZVPP[36] and were converged to 10^{-7} a.u. Because of the ∼200-atom size of the models, these energy calculations involved more than 5000 basis functions (e.g., 5478 basis functions for the chloride model). Both antiferromagnetic and ferromagnetic coupled states were computed. Also, energies were computed both for the actual optimized state and for the states where one electron was added or removed to enable calculation of vertical ionization energies and affinities used for reorganization energy calculations. In contrast, the relative ionization potentials were calculated from the fully relaxed geometries of both the oxidized and reduced states.

All these energies were computed both with B3LYP,[37−40] which is the most widely used density functional in current research,[41] and the TPSSh functional[42,43] with D3 dispersion correction[44] (60 computations with each functional). To study the effect of the dispersion correction, TPSSh energies were also computed without it. Computed energies of typical chemical reactions such as redox reactions, spin transitions, and bond dissociations depend almost linearly on the amount of HF exchange.[45−49] TPSSh was used due to its high accuracy for first-row transition metal systems,[50,51] including a range of experimental reaction enthalpies for challenging processes such as spin crossover of cobalt and iron systems[48,52] and metal−ligand bond dissociations.[53,54] The electronic energies can be found for reproducibility in the Supporting Information, Table S1.

To the computed electronic energies were added corrections for scalar-relativistic effects calculated with the Moloch module of Turbomole. Scalar-relativistic effects may amount to ∼10 kJ/mol or more even in first-row transition metals, and in particular for Cu, the effects can be non-negligible.[55] It was thus of interest to know how such corrections affect the coupling preferences (antiferromagnetic vs ferromagnetic), the reorganization energies, and relative ionization potentials of the TNCs. The energy gaps of these states are found in Supporting Information, Table S2, with representative spin populations and atomic charges found in Tables S3 and S4. Key optimized bond lengths are found in Tables S5 and S6, and the most relevant antiferromagnetic atomic spin values are collected in Table S7.

Ionization energies and reorganization energies were calculated from the dispersion-corrected, scalar-relativistic large basis set calculations as the optimized electronic energy of the oxidized state minus the same energy for the reduced states. Thus, for each cluster model and ligand type, both the II,I,I → II,II,I ionization and the II,II,I → II,II,II ionization were studied, corresponding to the energies of ionization to the three-electron and fully oxidized redox states, respectively. Reorganization energies were calculated from the standard procedure described by Ryde and co-workers[56,57] following the definition of the Marcus inner-sphere self-exchange reorganization energy,[58] that is, the difference between the vertical ionization energy and electron affinity of the reduced and oxidized states, or, analogously, the summed energy required to bring the oxidized and reduced states from their equilibrium geometry (fully optimized ground state energy) to the redox-pair geometry. This methodology has also been applied to the modeling of full reorganization energies for the noninhibited copper sites in laccase-like proteins.[59,60]

Harmonic frequencies were calculated for smaller models with 102 or 103 atoms as shown in Supporting Information, Figure S4, which include all imidazole rings fully but misses most second-sphere interactions. Zero-point energies and estimates of thermochemical state functions were calculated for the oxidized and one-electron reduced states with variable X using the freeh script of Turbomole, based on the harmonic frequencies to compute the vibrational state functions, as well as the rotation and translational degrees of freedom. These data are shown in Supporting Information, Table S8.

RESULTS AND DISCUSSION

Optimized Peroxo Intermediates. To validate the general model, the PI was computed since previous spectroscopic and density functional theory work has provided substantial insight into this intermediate: Notably, the conserved aspartate near the T2 site is important for stabilization of the PI and for binding of O_2.[61] Thus, this aspartate is required in quantum chemical modeling of the redox states and reorganization energies of laccases. The optimized structures of the three studied redox states of our 204-atom model are given in Figure 2, with the proximal aspartate shown to the right of the figures.

It is particularly notable that the T2 site is distorted planar, while the T3 sites are both distorted tetrahedral. The distortion is an indication of the two holes in the d shell since Cu(II) character is associated with Jahn−Teller instability. The smaller model used earlier[61] produced a μ_3-1,1,2 structure, that is, with one T3 copper coordinating both oxygen atoms. In the large model, all coppers have similar binding to only one oxygen: The difference lies in one of the T3 coppers, whereas the T2 copper important for studying relative effects of inhibiting ligands is in both models only in contact with one of the oxygens. It is also noticeable from Figure 2 that the O−O bond increases upon consecutive reduction, consistent with increased occupation of π^* orbitals that reduce the bond order on the reaction coordinate toward O−O cleavage. At the same time, the T2 Cu−X bond length increases significantly.

DOI: 10.1021/ic5021466
Inorg. Chem. 2015, 54, 476−483

In the present model, the T3 coppers differ, although there is also substantial valence delocalization. The spin densities are shown in Supporting Information, Table S7. For this model (OH^- (PI), II,II,I) indicates that one T3 copper (102Cu, corresponding to T3α in Solomon's notation[14]) has almost no hole density (−0.06), that is, resembles Cu(I), whereas the others represent Cu(II) with spin delocalized on ligands (−0.25, 0.50; notice the minus sign corresponding to antiferromagnetic coupling; the ferromagnetic coupled spins are given in Supporting Information, Table S3). The proximal aspartate most likely causes this difference in electron density on the T3 sites, since the negative charge is closer to the more oxidized 101Cu (i.e., T3β). These observations can explain the catalytic role of the Asp and were originally reported based on a smaller model by Yoon and Solomon[61] but are consistent also with the larger model studied here.

The computed one-electron reduced PI + e^- intermediate (II,I,I) has most hole density located at the T2 copper (0.28), leaving both T3 coppers of mainly Cu(I) character with little spin density. However, spin delocalization on ligands is substantial. Supporting Information, Table S5 shows the copper-ligand bond lengths of the optimized states: the bond between the T2 copper and the X ligand increases from ∼1.996 Å to 2.181 Å upon reduction to the PI + e^- intermediate, consistent with reduction of T2: The charge differences (Supporting Information, Table S4) supports that most electron density goes to ligands near the T2 copper, including X, which has its charge reduced by 0.3. Figure 3 shows the

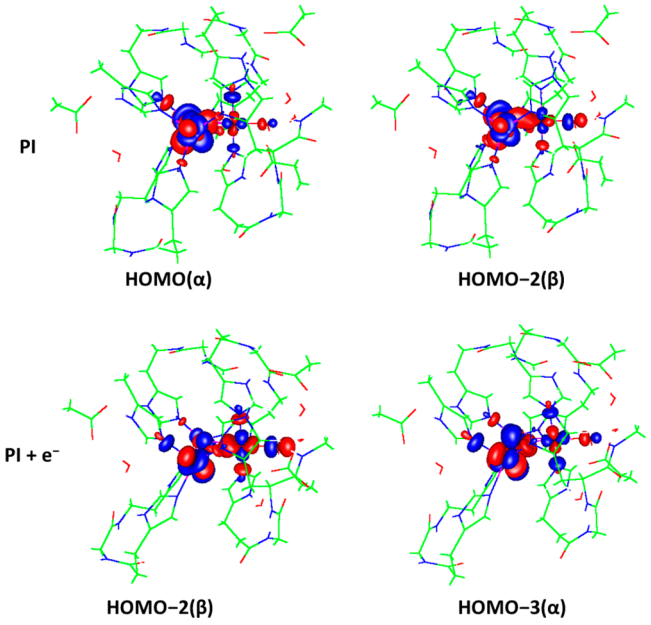

Figure 3. Molecular orbitals that have antibonding character with respect to the T2 Cu−X bond during reduction of the peroxo intermediate (PI). Figure made using gOpenMol.

molecular orbitals that accommodate the additional electron density affecting the T2 ligand. These orbitals are antibonding with respect to the T2 Cu−X but also include considerable Cu d-orbital character, peroxide character, and some histidine character.

Optimized Resting Oxidized and Halide-Bound States. We now turn to the discussion of primary focus of this work—the structures of the resting oxidized states with various ligands bound to the T2 copper. The spin densities of the models of the RO states with OH^- or H_2O bound are shown in the middle of Table S5. The redox state of the resting oxidized TNC is the (II,II,II) state, which needs to be reduced by T1 to follow the catalytic cycle:[14] These states are represented as (II,II,I) and (II,I,I). When computing the ferromagnetic and antiferromagnetic coupled states, the antiferromagnetic state is lower by 14 kJ/mol (scalar-relativistic corrected TPSSh-D3/def2-TZVPP, see Supporting Information, Table S2); this is consistent with SQUID experiments suggesting an antiferromagnetic RO state with a J coupling of ca. −7 kJ/mol (550 cm^{-1}).[62] Furthermore, the identified distorted square-planar coordination geometry of the T2 site is consistent with the consensus view based on MCD/EPR data;[63] ESEEM data indicate that the OH^- remains bound at activity relevant pH values, consistent with the model.[63] Both T3 coppers end up distorted tetrahedral or trigonal pyramidal, also in accordance with the consensus based on ligand-field transitions[14] (see also Cu−N bond lengths in Supporting Information, Table S7). The full XYZ coordinates are given in Supporting Information, Table S9.

Next, similar structures but with different ligands bound to T2 were computed. Examples of the molecular geometries of the optimized clusters of the resting oxidized states (X = Cl^- and OH^-) are given in Figure 4. The fully oxidized (II,II,II) and one-electron reduced (II,II,I) states had similar overall geometries and preserved bonds, although in particular the Cu−X bond elongates substantially upon reduction. This can be seen more clearly from the optimized bond lengths in Supporting Information, Table S6. Upon reduction of the fully oxidized state, the Cu−X bonds can be seen to elongate by 0.26 Å for X = Cl^-, 0.10 Å for X = F^-, 0.21 Å for H_2O, and 0.05 Å for OH^-, that is, most for the softer for the ligands. The Cu−Cu and Cu−N distances change by less than 0.1 Å, except with OH^-, where one of these bonds increases from 3.52 to 3.69 Å. Generally, the Cu−Cu bonds of these oxidized states are 3.0−3.5 Å. The Cu−O bonds from the coppers to the central oxide are also changed only marginally by one-electron reduction.

In contrast, when the one-electron-reduced (II,II,I) state is further reduced, major geometric changes occur for Cl^-, F^-, and H_2O, notably due to dissociation of the T2 ligand and accompanying changes in the cluster structure, as measured by the Cu−Cu distances (Table S6), which in some cases are substantially shortened or elongated, and in a few cases accompanied by trigonal copper coordination geometry. The OH^- ligand remains bound even in the two-electron reduced state. Experimentally, an as-isolated, less active "alternative resting state" has been observed in several laccase-like proteins, and reduction or heat can activate these alternative resting states.[25,26,28] Halides are natively present in the cells of host organisms used for protein expression, so that their binding to T2 copper could explain the observation of as-isolated alternative resting states. The computed result that two-electron reduction leads spontaneously to X dissociation is consistent with such an activation mechanism, which would also be possible by thermal dissociation.

Ionization Energies. To understand how T2 ligand binding may affect the electron-transfer properties of laccase-like proteins, the ionization energies and self-exchange reorganization energies were computed for the full models. These energies are sensitive to electrostatic effects in the second coordination sphere, justifying the use of large quantum mechanical models applied in this work; also, it provides a

DOI: 10.1021/ic5021466
Inorg. Chem. 2015, 54, 476−483

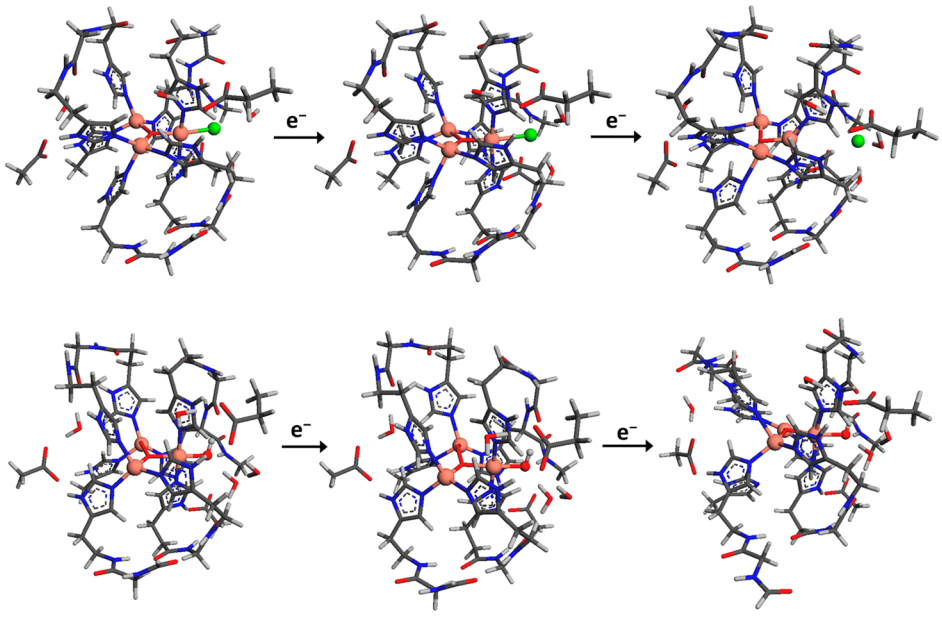

Figure 4. Geometry-optimized structures showing how two-electron reduction of the fully oxidized state causes the T2-ligand to dissociate (Cl^-, top, also seen for F^- and H_2O) or remain bound (OH^-, bottom).

Table 1. Ionization Energies Versus NHE and Reorganization Energies of Optimized Antiferromagnetically Coupled Trinuclear Clusters

		ionization energy −4.44 eV (more negative = easier to oxidize)		self-exchange reorganization energy (kJ/mol)	
ligand X	oxidation state	TPSSh-D3[a]/ def2-TZVPP	TPSSh-D3(rel)[b]/ def2-TZVPP	TPSSh-D3[a]/ def2-TZVPP	TPSSh-D3(rel)[b]/ def2-TZVPP
OH^-(PI)	II,II,I → II,II,II	−0.41	−0.55	38	37
	II,I,I → II,II,I	−2.18	−2.31	59	58
OH^-(RO)	II,II,I → II,II,II	−0.51	−0.69	57	54
	II,I,I → II,II,I	−1.84	−1.93	112	112
Cl^-	II,II,I → II,II,II	−0.04	−0.23	40	37
	II,I,I → II,II,I	−1.61	−1.68	152	154
F^-	II,II,I → II,II,II	−0.03	−0.23	27	25
	II,I,I → II,II,I	−1.53	−1.52	204	203
H_2O	II,II,I → II,II,II	0.04	−0.14	71	69
	II,I,I → II,II,I	−0.97	−1.04	144	147

[a]With Grimme's D3 dispersion correction. [b]With Cowan−Griffin scalar relativistic corrections.

relevant alternative to QM/MM calculations with necessarily smaller QM regions that use fixed force-field charges for the second sphere residues known to be vital to reactivity. The energies are shown in Table 1. The ionization energies have been corrected for a value of 4.44 eV to put the energies in a meaningful range relative to the standard hydrogen electrode. Note that real redox potentials include entropic effects that cannot be modeled with the large models studied here; thus the absolute values of the ionization energies do not relate to real redox processes. However, the *relative* ionization energies provide an estimate of the electronic contribution to the difference in half potential of the models. In this comparison, a more negative value means more easy to oxidize.

Scalar-relativistic values are shown in the fourth and sixth column of Table 1: For the ionization energies, they differ markedly from the noncorrected values by up to 0.2 eV, with a general tendency to make the ionization energies smaller, whereas for reorganization energies where two compensating states cancel in the calculation, they are less important: They change vertical excitation energies by up to ∼5 kJ/mol, but as these effects partly cancel due to the effect on the electron affinity and ionization energy, scalar-relativistic corrections change the total reorganization energies by a maximum of 3 kJ/mol (this is also why reorganization energies are very robust in general to e.g. chance in functional[59]). The correction for ionization energies is too large to be neglected, but as expected, for relative comparisons, it is less important due to cancellation of this systematic effect, a common reason why only such relative energies are meaningful.[41]

The corrections for zero-point energies and thermal effects were estimated from the rotation, translation and vibration state functions, the latter obtained from harmonic frequency calculations on the smaller models (Figure S4). As seen in Supporting Information, Table S8, the TΔS corrections can differ by up to 15 kJ/mol for antiferromagnetic vs ferromagnetic coupled states, consistent with previous findings.[41] In contrast, the zero point energies change by maximally 4 kJ/mol between these spin states. More importantly, the true redox potentials depend on the free energy of the redox states. Based on the antiferromagnetic coupled states, the TΔS contribution to the reduction half potential was estimated to be 12 kJ/mol for X = Cl^-, 25 kJ/mol for F^-, and 18 kJ/mol for

DOI: 10.1021/ic5021466
Inorg. Chem. 2015, 54, 476−483

OH^-. Zero-point energies were 7−8 kJ/mol smaller in the reduced states vs the oxidized counter parts, due to the elongated metal−ligand bonds and associated reduced zero-point energy upon one-electron reduction (Table S8). The total free energy corrections to the half potentials amounted to 0.19 V for X = Cl^-, 0.27 V for F^-, and 0.21 V for OH^-. Despite the partial entropy-energy compensation, these corrections are substantially smaller than the differences in computed ionization energies, and hence relative half potentials, discussed below.

The PI and RO models serve as reference systems for the noninhibited TNC. The PI model has a value of −0.55 eV for oxidation, whereas the scaled ionization energy of PI + e^- (II,I,I → II,II,I) is −2.31 eV. The (II,I,I) states generally have ionization energies lower by 1−2 eV due to the additional electron making it easier to remove an electron. From the point of view of the catalytic cycle, these larger values are the relevant ones, since the PI is required to be reduced by the T1 site to facilitate turnover.[14] The RO state model where OH^- is bound has a scaled ionization energy of −1.93 eV. If water were bound, which is not the case experimentally, this energy would almost 1 eV higher, to the effect of keeping electrons in the TNC.

The main observation is that with both Cl^- and F^- bound, the scaled ionization energies are substantially larger than for hydroxide, despite the same charge of the models. Thus, substitution of OH^- by halides significantly increases ionization energies by 0.3−0.4 eV, making it much harder to remove electrons from the TNC: The simple chemical explanation is that the halides are very electronegative and stabilize the electron density to the effect of increasing the ionization energies. Furthermore, F^- is more electronegative than Cl^- and thus has its ionization energy more increased, by 0.16 V for relativistic corrected values. Due to cancellation of systematic errors in such a relative comparison, the half potential is expected to increase also by hundred mV by halide binding to T2, and more so for fluoride binding. Shifting the half potential of the TNC is likely to impair the catalytic cycle, which relies on a balance between T1 reduction of the TNC and TNC reduction of dioxygen.

Reorganization Energies. A second important electron-transfer property that could be affected by halide binding is the reorganization energy of the TNC, defined as the summed energies required to distort the reduced state to the oxidized geometry and the oxidized state to the reduced geometry. Generally, an efficient electron transfer metal site should be accompanied by relatively small changes in geometry upon reduction and oxidation, reflecting a small reorganization energy and resulting higher rate of electron transfer:[58] Low reorganization energies have indeed been computed e.g. for important electron transfer sites such as cytochromes, blue copper proteins, and iron−sulfur clusters.[35,56,57] In contrast, the distance between the T1 and TNC will not change significantly by halide binding to T2, and thus, the donor−acceptor distance will not change and thus not affect the electron transfer process of the halide adducts.

The scalar-relativistic values are listed in the last column of Table 1. Since they have been computed for the full models, they include reorganization penalties associated with both first (inner) sphere and second sphere of the TNC; that is, they could be referred to as first-plus-second-sphere reorganization energies. The second coordination sphere is important in many metal-containing systems including laccases, where, for example, the mutagenesis of aspartates can remove activity.[30] Also, these residues can affect the T2 ligand binding and, thus, the relative electron transfer properties of the different species. Thus, including these in the full quantum chemical calculations seemed necessary.

The (II,II,II) resting oxidized states need to be reduced to enable formation of the PI from the reduced state.[14] Importantly, the II,I,I → II,II,I reductions associate with larger reorganization energies, due to the additional electron density in the highest occupied "antibonding" d-orbitals needing reorganization: Changes in these orbitals are associated with larger geometric changes due to their stronger interaction with the ligands. Also, this is the step where the T2 ligands can dissociate, as discussed above, to further increase the reorganization energy, potentially limiting the redox cycle; however, to put numbers to these effects, we also computed reorganization energies of the (II,II,I → II,II,II) step as shown in Table 1.

For the multicopper oxidase CueO, QM/MM calculations yielded total reorganization energies of 91−133 kJ/mol for electron transfer from T1 to PI, depending on method details.[59] This study also found inner-sphere (i.e., first coordination-sphere) reorganization energies of ∼57 kJ/mol for the T1 site and ∼61 kJ/mol for the PI state of the TNC using isolated quantum models but only 12 and 22 kJ/mol contribution based on the QM/MM calculations.[59] In the protein, the geometry changes of the copper sites will be damped by protein polarization and structural constraints, causing the sites to deviate less in geometry during the redox process, giving smaller copper-site contributions to the total protein reorganization energies. In contrast, the isolated QM cluster value represents the free cluster, not the cluster in the protein. Still, it is also an accomplishment of the protein to dampen the structural changes in addition to the second, larger electrostatic polarization effect on reorganization energy.

For comparison to these previous results, the self-exchange reorganization energy for the larger quantum-mechanical PI model used here is 58 kJ/mol (TPSSh, scalar-relativistic corrected), which is quite similar to previous cluster values.[59] Since we are not aiming for absolute accuracy but the particular mechanism of halide inhibition, both the protein's direct effect and the structural damping effect can be assumed constant during halide binding, whereas the second sphere is not modeled classically as in QM/MM due to direct electronic interactions with the T2 ligand, central to the present work, and the copper-binding histidines.[14]

For the critical II,I,I → II,II,I reduction, the reorganization energy reaches 112 kJ/mol for the OH^- bound RO state. These values are as required smaller than but constitute a significant fraction of the total reorganization energy obtained from thermodynamic data of electron transfer by Farver et al. for a fungal and the lacquer tree laccase (∼135 and 172 kJ/mol)[16] and substantially larger than the protein-constrained cluster values as discussed above.[59]

However, with Cl^- or F^- bound, the reorganization energy for the rate-limiting reduction increases to 154 and 203 kJ/mol, respectively, notably in line with the experimental order of inhibitory effect $F^- > Cl^-$. It can be rationalized by the changes in geometry associated with this redox step, where the Cu−X bond lengths change substantially due to the accommodation of electron density in the electronegative halides (Table S6 in Supporting Information). These reorganization energies for the

DOI: 10.1021/ic5021466
Inorg. Chem. 2015, 54, 476−483

(II,I,I),(II,II,I) redox pair are substantially larger and thus critical to slow reduction of the resting states.

In principle, F^- could inhibit more because it has easier access through laccase water channels, due to its general effect on disruption of laccase backbone integrity by formation of strong hydrogen bonds[64] or due to stronger binding to the T2 site preventing water/oxygen binding and release.[14] However, the present computations show that the actual electron-transfer properties are likely to be directly impaired. This can explain why alternative resting states with reduced activity are only reactivated after being subject to strong reducing agents to produce the full reduced states, which then readily enters the catalytic cycle.[28]

It has also been observed that laccase-like proteins are less inhibited by halides at higher pH, probably due to competition between OH^- and F^-/Cl^-.[66,65] For the relevant "slow" second reduction of the RO state, the reorganization energy is indeed smaller for OH^- (112 kJ/mol) than for Cl^- (154 kJ/mol). Importantly, this difference is because, due to less electronegativitiy and thus less electron density retained on hydroxide relative to the halides, the hydroxide contains less dissociated ion character and thus does not dissociate during computational reduction. These findings are consistent with laccases having higher chloride tolerance at high pH due to OH^-/Cl^- competition;[65] that is, a larger fraction of the laccases have OH^- bound despite the chloride presence, and these exhibit smaller reorganization energies for the critical reduction of the resting states.

CONCLUSIONS

We have studied computationally for the first time in systematic detail possible mechanisms behind halide inhibition of laccase-like proteins. The computed reorganization energy is substantially larger with F^- bound, followed by Cl^- and hydroxide. The results provide an explanation for experimental observations of halide inhibition, including the order of inhibition $F^- > Cl^-$,[66] directly related to electron-transfer parameters. The notable shifts in half potentials and increased reorganization energies result from the electronegativity of the halides binding to T2. Although other mechanisms were not studied, such as binding strengths, channel accessibility due to anion size, or general disruption of channels by backbone interactions, the findings provide simple suggestions for inhibition that relate directly to the redox chemistry.

One of the main reasons for the low reorganization energies of TNCs is the fact that the reducing electrons are delocalized over the cluster; this has the effect of reducing repulsion between the redox electrons and the ligand lone pairs, so that metal−ligand distances are less variable during redox reaction. When hydroxide is bound to T2, its moderate electronegativity preserves its binding during the studied redox states. However, when the very electronegative halides bind, we find that they must dissociate during reduction to the full reduced state already during the second (II,II,I) reduction, causing further increases in reorganization energies. Selective reduction or thermal dissociation of T2 ligands by heating offer ways to activate laccase-like proteins, consistent with the mechanisms described in this work.

ASSOCIATED CONTENT

Supporting Information

Electronic energies for optimized states and the energy gap between ferromagnetic and antiferromagnetic coupled states; atomic spin of ferromagnetic coupled states; Mulliken charges of key atoms; optimized Cu−N bonds; optimized Cu−Cu and Cu−O bonds; atomic spin in antiferromagnetic coupled clusters; optimized structures of the (II,II,I) 1-reduced states or the RO states; molecular orbitals of the PI and reduced PI; small models used for computing frequencies; zero point energies and thermodynamic state functions; and XYZ coordinates for optimized models. This material is available free of charge via the Internet at http://pubs.acs.org.

AUTHOR INFORMATION

Corresponding Author

*E-mail: kpj@kemi.dtu.dk.

Notes

The authors declare no competing financial interest.

ACKNOWLEDGMENTS

This research has been supported by the Danish Center for Scientific Computing (Grant No. 2012-02-23) and by The Danish Council for Independent Research | Technology and Production Sciences (*FTP*) (Grant No. 10-082488).

REFERENCES

(1) Grass, G.; Rensing, C. *Biochem. Biophys. Res. Commun.* **2001**, *286*, 902−908.
(2) De Silva, D.; Davis-Kaplan, S.; Fergestad, J.; Kaplan, J. *J. Biol. Chem.* **1997**, *272*, 14208−14213.
(3) Koikeda, S.; Anso, K.; Kaji, H.; Inoue, T.; Murao, S.; Takeuchi, K.; Samejima, T. *J. Biol. Chem.* **1993**, *268*, 18801−18809.
(4) Xu, F.; Shin, W.; Brown, S. H.; Wahleithner, J. A.; Sundaram, U. M.; Solomon, E. I. *Biochim. Biophys. Acta* **1996**, *1292*, 303−311.
(5) Quintanar, L.; Stoj, C.; Taylor, A. B.; Hart, P. J.; Kosman, D. J.; Solomon, E. I. *Acc. Chem. Res.* **2007**, *40*, 445−452.
(6) Rodríguez, C. S.; Herrera, J. L. T. *Biotechnol. Adv.* **2006**, *24*, 500−513.
(7) Reiss, R.; Ihssen, J.; Richter, M.; Eichhorn, E.; Schilling, B.; Thöny-Meyer, L. *PLoS One* **2013**, *8*, e65633.
(8) Martins, L. O.; Soares, C. M.; Pereira, M. M.; Teixeira, M.; Costa, T.; Jones, G. H.; Henriques, A. O. *J. Biol. Chem.* **2002**, *277*, 18849−18859.
(9) Wesenberg, D.; Kyriakides, I.; Agathos, S. N. *Biotechnol. Adv.* **2003**, *22*, 161−187.
(10) Mayer, A. M.; Staples, R. C. *Phytochemistry* **2002**, *60*, 551−565.
(11) Piscitelli, A.; Del Vecchio, C.; Faraco, V.; Giardina, P.; Macellaro, G.; Miele, A.; Pezzella, C.; Sannia, G. *C. R. Biol.* **2011**, *334*, 789−794.
(12) Stoilova, I.; Krastanov, A.; Stanchev, V. *Adv. Biosci. Biotechnol.* **2010**, *1*, 208−215.
(13) Madhavi, V.; Lele, S. S. *Bioresources* **2009**, *4*, 1694−1717.
(14) Solomon, E. I.; Heppner, D. E.; Johnston, E. M.; Ginsbach, J. W.; Cirera, J.; Qayyum, M.; Kieber-Emmons, M. T.; Kjaergaard, C. H.; Hadt, R. G.; Tian, L. *Chem. Rev.* **2014**, *114*, 3659−3853.
(15) Rulísek, L.; Ryde, U. *Coord. Chem. Rev.* **2013**, *257*, 445−458.
(16) Farver, O.; Wherland, S.; Koroleva, O.; Loginov, D. S.; Pecht, I. *FEBS J.* **2011**, *278*, 3463−3471.
(17) Malkin, R.; Malmström, B. G.; Vinngaard, T. *FEBS Lett.* **1968**, *89*, 50−54.
(18) Naqui, A.; Varfolomeev, S. D. *FEBS Lett.* **1980**, *113*, 157−160.
(19) Torres-Salas, P.; Mate, D. M.; Ghazi, I.; Plou, F. J.; Ballesteros, A. O.; Alcalde, M. *ChemBioChem* **2013**, *14*, 934−937.
(20) Gunne, M.; Urlacher, V. B. *PLoS One* **2012**, *7*, e52360.
(21) Sulistyaningdyah, W. T.; Ogawa, J.; Tanaka, H.; Maeda, C.; Shimizu, S. *FEMS Microbiol. Lett.* **2004**, *230*, 209−214.
(22) Claus, H. *Arch. Microbiol.* **2003**, *179*, 145−150.
(23) Santhanam, N.; Vivanco, J. M.; Decker, S. R.; Reardon, K. F. *Trends Biotechnol.* **2011**, *29*, 480−489.

DOI: 10.1021/ic5021466
Inorg. Chem. 2015, 54, 476−483

(24) Hullo, M. F.; Moszer, I.; Danchin, A.; Martin-Verstraete, I. *J. Bacteriol.* **2001**, *183*, 5426−5430.
(25) Sakurai, T.; Zhan, L.; Fujita, T.; Kataoka, K.; Shimizu, A.; Samejima, T.; Yamaquchi, S. *Biosci. Biotechnol. Biochem.* **2003**, *67*, 1157−1159.
(26) Brander, S.; Mikkelsen, J. D.; Kepp, K. P. *PLoS One* **2014**, *9*, e99402.
(27) Mollania, N.; Khajeh, K.; Ranjbar, B.; Hosseinkhani, S. *Enzyme Microb. Technol.* **2011**, *49*, 446−452.
(28) Kjaergaard, C. H.; Durand, F.; Tasca, F.; Qayyun, M. F.; Kauffman, B.; Gounel, S.; Suraniti, E.; Hodgson, K. O.; Hedman, B.; Mano, N.; Solomon, E. I. *J. Am. Chem. Soc.* **2012**, *134*, 5548−5551.
(29) Enguita, F. J.; Martins, L. O.; Henriques, A. O.; Carrondo, M. A. *J. Biol. Chem.* **2003**, *278*, 19416−19425.
(30) Quintanar, L.; Stoj, C.; Wang, T. P.; Kosman, D. J.; Solomon, E. I. *Biochemsitry* **2005**, *44*, 6081−6091.
(31) Rulisek, L.; Solomon, E. I.; Ryde, U. *Inorg. Chem.* **2005**, *44*, 5612−5628.
(32) Ahlrichs, R.; Bär, M.; Häser, M.; Horn, H.; Kölmel, C. *Chem. Phys. Lett.* **1989**, *162*, 165−169.
(33) Weigend, F.; Ahlrichs, R. *Phys. Chem. Chem. Phys.* **2005**, *7*, 3297−3305.
(34) Klamt, A.; Jonas, V.; Bürger, T.; Lohrenz, J. C. W. *J. Phys. Chem. A* **1998**, *102*, 5074−5085.
(35) Jensen, K. P. *J. Inorg. Biochem.* **2008**, *102*, 87−100.
(36) Schäfer, A.; Horn, H.; Ahlrichs, R. *J. Chem. Phys.* **1992**, *97*, 2571−2577.
(37) Becke, A. D. *J. Chem. Phys.* **1993**, *98*, 5648−5652.
(38) Lee, C.; Yang, W.; Parr, R. G. *Phys. Rev. B* **1988**, *37*, 785−789.
(39) Stephens, P. J.; Devlin, F. J.; Chabalowski, C. F.; Frisch, M. J. *J. Phys. Chem.* **1994**, *98*, 11623−11627.
(40) Kim, K.; Jordan, K. D. *J. Phys. Chem.* **1994**, *98*, 10089−10094.
(41) Kepp, K. P. *Coord. Chem. Rev.* **2013**, *257*, 196−209.
(42) Tao, J.; Perdew, J. P.; Staroverov, V. N.; Scuseria, G. E. *Phys. Rev. Lett.* **2003**, *91*, 146401.
(43) Perdew, J. P.; Tao, J.; Staroverov, V. N.; Scuseria, G. E. *J. Chem. Phys.* **2004**, *120*, 6898−6911.
(44) Grimme, S.; Antony, J.; Ehrlich, S.; Krieg, H. *J. Chem. Phys.* **2010**, *132*, 154104.
(45) Reiher, M. *Inorg. Chem.* **2002**, *41*, 6928−6935.
(46) Paulsen, H.; Duelund, L.; Winkler, H.; Toftlund, H.; Trautwein, A. X. *Inorg. Chem.* **2001**, *40*, 2201−2203.
(47) Daku, L. M. L.; Vargas, A.; Hauser, A.; Fouqueau, A.; Casida, M. E. *ChemPysChem* **2005**, *6*, 1393−1410.
(48) Jensen, K. P.; Cirera, J. *J. Phys. Chem. A* **2009**, *113*, 10033−10039.
(49) De Visser, S. P.; Quesne, M. G.; Martin, B.; Comba, P.; Ryde, U. *Chem. Commun.* **2014**, *50*, 262−282.
(50) Furche, F.; Perdew, J. P. *J. Chem. Phys.* **2006**, *124*, 044103.
(51) Zhao, Y.; Truhlar, D. G. *J. Chem. Phys.* **2006**, *124*, 224105.
(52) Matouzenko, G. S.; Borshch, S. A.; Schünemann, V.; Wolny, J. A. *Phys. Chem. Chem. Phys.* **2013**, *15*, 7411−7419.
(53) Jensen, K. P. *Inorg. Chem.* **2008**, *47*, 10357−10365.
(54) Kepp, K. P.; Dasmeh, P. *J. Phys. Chem. B* **2013**, *117*, 3755−3770.
(55) Jensen, K. P.; Roos, B. O.; Ryde, U. *J. Chem. Phys.* **2007**, *126*, 014103.
(56) Olsson, M. H.; Ryde, U.; Roos, B. O. *Protein Sci.* **1998**, *7*, 2659−2668.
(57) Sigfridsson, E.; Olsson, M. H. M.; Ryde, U. *Inorg. Chem.* **2001**, *40*, 2509−2519.
(58) Marcus, R. A.; Sutin, N. *Biochim. Biophys. Acta* **1985**, *811*, 265−322.
(59) Shleev, S.; Andoralov, V.; Falk, M.; Reimann, C. T.; Ruzgas, T.; Srnec, M.; Ryde, U.; Rulisek, L. *Electroanalysis* **2012**, *24*, 1524−1540.
(60) Hu, L.; Farrokhnia, M.; Heimdal, J.; Shleev, S.; Rulisek, L.; Ryde, U. *J. Phys. Chem. B* **2011**, *115*, 13111−13126.
(61) Yoon, J.; Solomon, E. I. *J. Am. Chem. Soc.* **2007**, *129*, 13127−13136.
(62) Solomon, E. I.; Sundaram, U. M.; Machonkin, T. E. *Chem. Rev.* **1996**, *96*, 2563−2606.
(63) Quintanar, L.; Yoon, J.; Aznar, C. P.; Palmer, A. E.; Andersson, K. K.; Britt, R. D.; Solomon, E. I. *J. Am. Chem. Soc.* **2005**, *127*, 13832−13845.
(64) Christensen, N. J.; Kepp, K. P. *PLoS One* **2013**, *8*, e61985.
(65) Xu, F. *J. Biol. Chem.* **1997**, *272*, 924−928.
(66) Mate, D. M.; Gonzalez-Perez, D.; Kittl, R.; Ludwig, R.; Alcalde, M. *BMC Biotechnol.* **2013**, *13*, 38.

DOI: 10.1021/ic5021466
Inorg. Chem. 2015, 54, 476−483